Chemical and physical analysis of natural gas hydrate from the JAPEX/JNOC/GSC Mallik 2L-38 gas hydrate research well

C.A. Tulk[1], C.I. Ratcliffe[1], and J.A. Ripmeester[1]

Tulk, C.A., Ratcliffe, C.I., and Ripmeester, J.A., 1999: Chemical and physical analysis of natural gas hydrate from the JAPEX/JNOC/GSC Mallik 2L-38 gas hydrate research well; in *Scientific Results from JAPEX/JNOC/GSC Mallik 2L-38 Gas Hydrate Research Well, Mackenzie Delta, Northwest Territories, Canada, (ed.) S.R. Dallimore, T. Uchida, and T.S. Collett; Geological Survey of Canada, Bulletin 544, p. 251–262.*

Abstract: Gas hydrate samples from the JAPEX/JNOC/GSC Mallik 2L-38 gas hydrate research well were analyzed on both macroscopic and molecular scales using several complementary experimental techniques. These included gas volume analysis, thermogravimetric analysis, precision gas analysis, powder X-ray diffraction, differential scanning calorimetry, Fourier transform infrared spectroscopy, and Raman Spectroscopy. Powder X-ray diffraction indicated that the samples were Structure I gas hydrate. Enclathrated gas species were identified to be mostly methane (98–100%); however, some samples contained significant amounts of heterogeneously dispersed propane and carbon dioxide (at least 1.5–2.0%). These samples were found to be significantly more stable than samples containing methane only. In addition, Raman spectra indicate subtle variations in the cage occupancies of the mixed gas hydrate as compared to those in pure methane hydrate.

Résumé : Des échantillons d'hydrates de gaz provenant du puits de recherche sur les hydrates de gaz JAPEX/JNOC/GSC Mallik 2L-38 ont été analysés à des échelles macroscopique et moléculaire à l'aide de plusieurs techniques expérimentales complémentaires, notamment l'analyse volumétrique du gaz, l'analyse thermogravimétrique, l'analyse de précision du gaz, la diffraction des rayons X sur poudre, la calorimétrie à balayage différentielle, la spectroscopie infrarouge par transformée de Fourier et la spectroscopie Raman. La diffraction des rayons X sur poudre indique que les échantillons étaient des hydrates de gaz de Structure I. On a démontré que les espèces de gaz encagés dans un clathrate étaient pour la plupart du méthane (de 98 à 100 %). Toutefois, certains échantillons contenaient d'importantes quantités de propane et de dioxyde de carbone dispersés d'une manière hétérogène (au moins 1,5 à 2,0 %). On a observé que ces échantillons étaient de loin plus stables que les échantillons ne renfermant que du méthane. En outre, les spectres Raman montrent de légères variations dans l'occupation des cages par les hydrates de gaz mixtes par rapport à celles par l'hydrate de méthane pur.

[1] Steacie Institute for Molecular Sciences, National Research Council of Canada, 100 Sussex Drive, Ottawa, Ontario, Canada K1A 0R6

SCOPE OF PAPER

This paper provides a detailed discussion of the physical and chemical analysis of gas hydrate contained in cored material collected from the JAPEX/JNOC/GSC Mallik 2L-38 gas hydrate research well drilled on the Mackenzie Delta, Northwest Territories, Canada, in the winter of 1998. Core samples were collected by members of the Geological Survey of Canada and were shipped to the laboratory at the Steacie Institute for Molecular Science, National Research Council of Canada in Ottawa for analysis.

INTRODUCTION

Natural gas hydrate has now been recognized as an important mineral resource with implications both for the Earth's future energy supply and global climate change (Kvenvolden, 1994). A great deal of information is still needed in order to obtain realistic estimates of the Earth's gas hydrate budget, to predict the locations of gas hydrate deposits, and to understand the natural processes leading to gas hydrate formation and decomposition (Sloan, 1998). A feature of singular importance of gas hydrate is its tremendous capacity for storing small molecules such as the natural gas components. This feature arises from the general nature of clathrate hydrate, of which natural gas hydrate is a subgroup. It is formed by water molecules which hydrogen-bond in a tetrahedral manner, much as in ice, but in a variety of ways to fill space by forming cages that share faces (Jeffrey, 1996). The hydrate cage structure is known as the host lattice. As the empty clathrate is unstable with respect to ice, these open structures are stabilized by guest molecules trapped within the cages. All molecules in the size range from ~ 0.38 nm (argon) to 0.92 nm (e.g. 2,2-Dimethylpentane) are suitable candidates for guests, the only stipulation other than size being that the guest molecules must be sufficiently hydrophobic (Davidson, 1973). Also, there are minimum cage-occupancy requirements for clathrate hydrate stability (van der Waals and Platteeuw, 1959).

Suitable guest molecules for the natural gas hydrates are natural gas hydrocarbons such as methane, ethane, propane, isobutane and other light hydrocarbons, carbon dioxide, nitrogen, oxygen, H_2S, traces of noble gases, etc. The detailed structure of the gas hydrate is a function of the nature of the guest molecules present and the partial pressure of each guest-molecule type. Gas hydrate is known to form three distinct crystallographic structures. Structure I is crystallographically cubic, space group Pm3n, and contains 46 water molecules per unit cell with $a \sim 12$ Å, pure methane gas forms this structure (Jeffrey, 1996; Davidson, 1994). Structure II is also crystallographically cubic, space group Fd3m, and contains 136 water molecules per unit cell with $a \sim 17$ Å, pure propane gas and propane-methane mixture usually form this structure (Jeffrey, 1996; Davidson, 1994). Structure H is crystallographically hexagonal, space group P6/mmm, and contains 34 water molecules per unit cell with $a \sim 12$ Å and $b \sim 10$ Å, this structure is usually formed by larger guest molecules such as neohexane and isopentane, which occupy the large cages in combination with smaller molecules such as CH_4 or CO_2 that are known as 'help-gases' and stabilize the lattice by occupying smaller cages (Ripmeester et al., 1987; Udachin et al., 1997). Evidence for each of these structure types has been reported as occurring naturally, with structures II (Davidson et al., 1986) and H (Sassen and Macdonald, 1994) recovered from the Gulf of Mexico and Structure I from the Blake Ridge (Davidson et al., 1986; Handa et al., 1997).

Previously we have applied molecular-scale techniques to natural gas hydrate samples in order to determine structure and composition. The work reported here will affirm that structure and guest-molecule composition play key roles in determining the details of the formation and decomposition behaviour of natural gas hydrate. This information is of paramount importance both for the development of economic gas-recovery schemes from gas hydrate deposits, as well as for assessing the natural processes leading to release or capture of greenhouse gases such as methane and carbon dioxide (Kvenvolden, 1994).

OVERALL SAMPLE ANALYSIS

Samples and experiments

This paper reports several preliminary experimental studies of the natural gas hydrate recovered from the Mallik 2L-38 gas hydrate research well that was drilled on the Mackenzie Delta in the winter of 1998. In all, 11 core samples were recovered from gas-hydrate-bearing sediment at depths between 898.45 and 913.90 m (all depths were measured from kelly bushing [8.31 m above sea level]). These samples were stored in liquid nitrogen immediately upon recovery (T = 77 K, well below the equilibrium dissociation temperature at atmospheric pressure of gas hydrate (Handa et al., 1997; Handa, 1986)). The samples were transported in liquid nitrogen to the National Research Council of Canada laboratories in Ottawa. Initial inspection revealed that the core samples were composed of approximately 85% consolidated sand of variable grain size (from fine grained sand, ~100 μm, to pebbly sand, ~1–3 mm), hereafter referred to as the background sand matrix, held together by a mixture of ice and gas hydrate, which constitutes approximately 15% of total mass. Unlike other natural gas hydrate samples studied by this lab, there was very little visible ice/gas hydrate present. This low concentration of mostly invisible gas hydrate presented several challenges during the sample analysis. The next section illustrates those challenges and the analysis of the bulk properties (gas hydrate/ice + background sand matrix without separation of the two) of each of the 11 samples using quantitative gas-volume analysis, thermogravimetric analysis, and precision gas analysis/mass spectroscopy. In the subsequent section, the procedure used to separate the background sand matrix from the gas hydrate/ice, while keeping the gas hydrate within its stability field, is described and a more detailed molecular-level analysis of gas hydrate/ice material from two core samples is reported.

Gas-volume analysis

The volume of gas contained per gram of sample (gas hydrate + ice + background sand matrix) was measured using a vacuum line and calibrated gas bulb. The procedure used for each of the 11 core samples is as follows. The core sample was removed from liquid nitrogen (lN$_2$) storage, placed in a lN$_2$ bath and subdivided into approximately 1 g chunks. Several such chunks were placed in a cold (77 K) glass tube, which was closed at one end and fitted with a ground-glass vacuum joint at the other. The sample used thus provided a representative subsection of each core sample. The tube was then placed on the vacuum line with the closed end submerged in a lN$_2$ bath. Excess liquid was removed by pumping for several minutes until the line pressure was less than 4.0×10^{-4} Torr. The lN$_2$ bath was then removed and the temperature was increased and held isothermally at 113 K by using an isopentane cryogenic bath. Pumping at this temperature for 30 min resulted in the efficient removal of all non-enclathrated gases, including nitrogen adsorbed on the ice/gas hydrate surface (Tulk et al., 1999). Subsequently, the sample temperature was reduced to 77 K by reapplying the liquid nitrogen bath. Once equilibrium was reached, the temperature was raised continuously from 77 to 293 K and the pressure monitored continuously and recorded. The total amount of gas released was then calculated using (P, V, T) analysis by condensing the gas into a calibrated volume and slowly heating the volume to room temperature (294 K). (The gas pressure was corrected for the partial pressure of water produced by the ice and water.) The mass of the wet and dry sand was measured on an analytical balance (± 0.2 mg). The total amounts of gas released per unit mass and core depth for each sample is reported in Table 1. This information provides good baseline data and was used to identify samples suitable for further studies.

The water content of each sample was also measured by thermogravimetric analysis (TGA) to determine if any water was held in a *bound* state (i.e. adsorbed onto any hydrophilic minerals and thus unlikely to participate in significant gas hydrate formation). Samples were removed from liquid nitrogen and placed in a small glass cell fitted with a one-way gas-release valve. The sample temperature was raised to 294 K and the one-way valve allowed the gas to be released, avoiding pressure buildup, while preventing the condensation of atmospheric water onto the cold sample. The cell was constructed such that the dead space above the sample was minimized. The wet sand was then loaded at room temperature into an aluminum TGA sample pan and quickly placed in the sample chamber. The sample temperature was held isothermally at 303 K for ~ 60 min and the sample mass continuously monitored. This allowed the excess unbound water to be removed by the ultra-dry nitrogen purge gas. Subsequently, the temperature was ramped to 473 K, and again the sample mass was continuously monitored. Bound water would be evident as a loss of mass as the sample temperature was increased. A representative plot of a TGA scan collected from core sample A2 (the naming scheme follows that of Table 1) is presented in Figure 1. It is evident that no significant portion of the water in any of the 11 core samples was held in a bound state.

Table 1. Core sample gas composition.

Sample number	Depth (cm)/ description	Gas vol/mass (mmol/g) ±0.05	Water content (%) ±0.3
B1	91360-91366 gravelly sand	0.2	9.6
B2	91325-91340 pebbly sand	0.4	15.2
B3	90075-90080 end of core	0.03	14.5
B4	89845 medium grain	0.2	16.0
B5	89880 medium grain	0.6	14.6
B6	90080 end of core	0.1	10.5
A1	90488-90505 medium grain	0.1	17.6
A2	89850 medium grain	0.5	14.8
A4	91382-91390 sandy pea gravel	0.04	19.3
A5	91350 sandy pea gravel	0.1	9.0
A6	90505-90515 medium grain	0.1	17.4

Note that the gas-content values reported above represent the total amount of enclathrated gas present in the samples. The above data only identifies candidates for further study. The water content was measured using a digital balance before and after drying the samples and is believed to be more accurate than the TGA results.

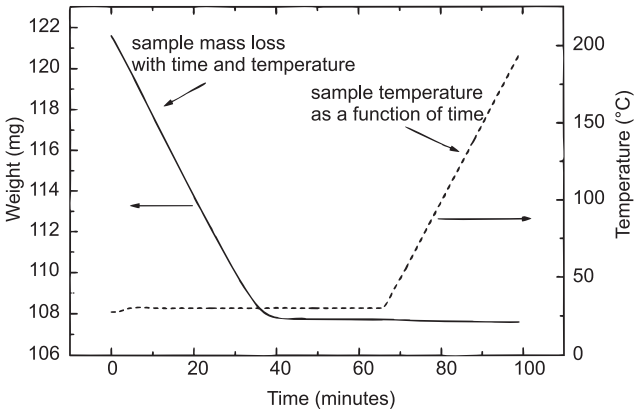

Figure 1. *Thermogravimetric analysis of the free vs. bound water content. The solid line represents the sample mass and is associated with the left-hand y axis and the dashed line represents the sample temperature and is associated with the right-hand y axis. No sample mass was lost as the temperature.*

The profile of the gas released as a function of temperature for each of the core samples is given in Figure 2 (the naming scheme corresponds to that given in Table 1). The y-axis units are given in fraction of the gas hydrate decomposed and have been calculated from the vacuum-line pressure recorded during continuous heating. All the data presented have been corrected for the partial pressure of water vapour. The average heating rate during the warmup was 1.8 K/min, and therefore the system can be considered to be very close to equilibrium at all times.

It is understood that dissociation of bulk gas hydrate (gas hydrate grains larger then 2 mm) by isothermal pressure drop at temperatures below 273 K may result in a self-preservation process. This process is facilitated by the formation of an *ice jacket* that structurally supports the internal pressure at a level required to stabilize the underlying gas hydrate. To date, very few scientific studies have investigated self-preservation in porous material (Handa and Stupin, 1992). The inset of Figure 2 illustrates a single dissociation profile and nicely shows the self-preservation effect. The slight increase in pressure at 0°C shows the release of gas from self-preserved gas hydrate material as the ice jacket melts, and confirms that the system is very close to equilibrium during the heating process. It is noteworthy that approximately 85–95% of the gas hydrate dissociated in the temperature interval between -196 and -50°C. Samples that have been stored in liquid nitrogen must be handled below 173 K to insure that no gas hydrate decomposes before testing. In fact, the results shown in Figure 2 suggest that the self-preservation process cannot be relied upon to preserve significant portions of gas hydrate in porous media formed by macroscopic sand grains. The average grain size is roughly 0.3 mm (Wright et al., 1999) which if assumed to be spherical particles, will give an average pore diameter of approximately 0.046 mm. It is not likely that such a large pore size will significantly affect the equilibrium dissociation P-T conditions of the gas hydrate, a point made previously (Wright et al., 1999). This, however, does not mean that these large pores do not significantly affect the self-preservation process.

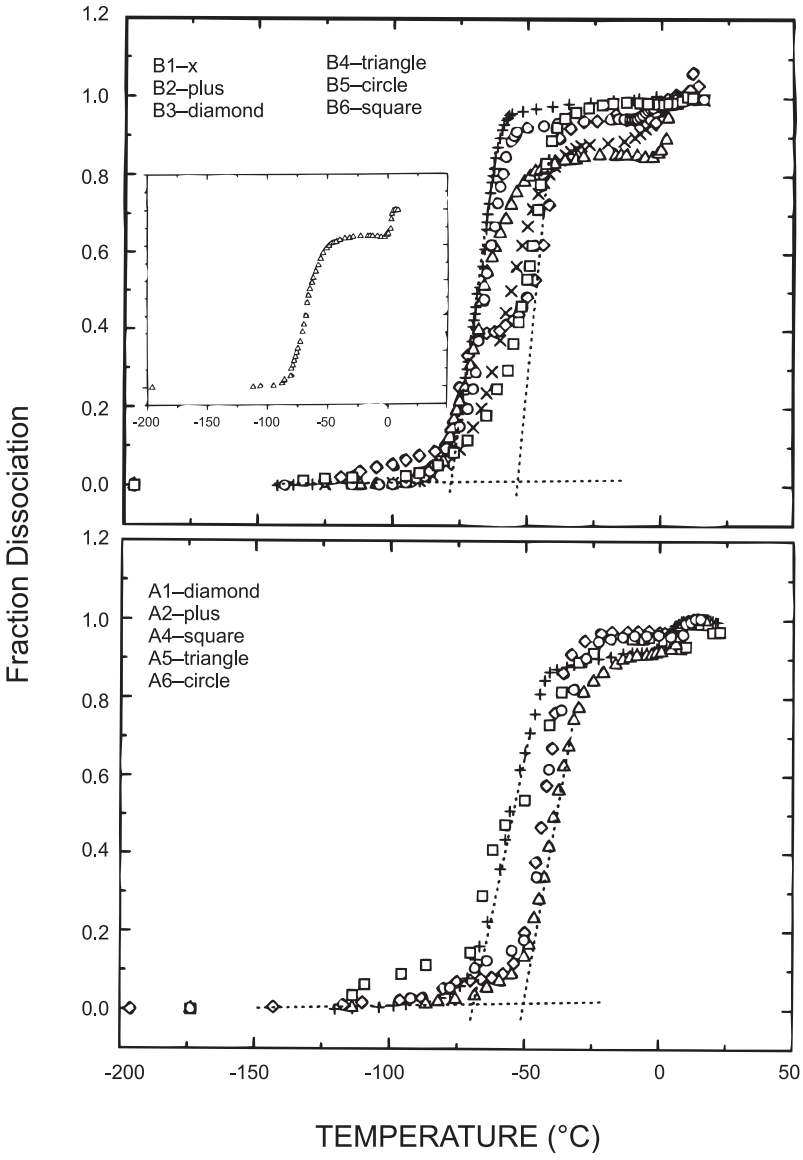

Figure 2.

Gas hydrate decomposition (vacuum-line pressure increase) as a function of temperature. The gas hydrate dissociation temperature was found to vary between 193 and 223 K. The inset shows the self preservation effect, note the plateau between –50 and 0°C, then the final gas release as the ice melts.

Perhaps the most important feature of Figure 2 is a slight variation in the gas hydrate dissociation temperature among the various core samples; the phenomenon will be discussed along with calorimetric data presented in 'Thermal analysis of the decomposition process'. The gas hydrate dissociation temperature (calculated from the profiles presented in Fig. 2 by manually determining the intersection of the extended baseline prior to dissociation with the tangent to the profile at approximately 50% dissociation) is bracketed between approximately -80 and -50°C. Since the self-preservation process results only after the initial gas hydrate dissociation and ice-jacket formation, and is evident only after the ice jacket melts at 0°C, the initial gas release, between -80 and -50°C, most likely represents the gas hydrate/ice/gas equilibrium. It is interesting to note that the dissociation temperature and pressure of mixed gas hydrate of methane and other gases can vary widely depending on the details of the gas composition (Sloan, 1998). The occurrence of other gases is likely the source of this variation, which may lead to considerable variability in the way that gas hydrate behaves. High-temperature equilibrium conditions for gas mixtures have been compiled and documented (Sloan, 1998). The profile for sample B3, represented by open diamonds in Figure 2, is of particular interest as it shows three distinct steps in the dissociation process: 1) the sample begins to dissociate at low temperature, approximately -80°C, then 2) shows a stable plateau region between -70 and -55°C, then 3) exhibits a second dissociation step beginning at approximately -50°C. This sample nicely indicates the variation in the stability conditions of the gas hydrate and provides good evidence of their heterogeneous nature even for subsamples from within the same core section.

Gas analysis

Detailed knowledge of the composition of the enclathrated gas is not only required for understanding the gas hydrate stability conditions, but is also required for any accurate modelling of the geochemical processes involved in the gas hydrate formation and evolution. Preliminary identification of the guest species present in each of the 11 Mallik 2L-38 core samples was provided by measuring the molecular weights of the dissociated gases using an UTI 100C precision mass analyzer. The molecular weights of the various species present were identified — this helped to determine uniquely the guest species present. At this point no attempts were made to determine quantitatively the relative fractions of each species present. This is in part due to the fact that many of the peaks in the cracking pattern of each gas species overlap, thus making absolute species identification difficult and the preparation of calibration curves impossible. The absolute identification of the guest species was accomplished with infrared spectroscopy.

Each of the 11 core samples were studied individually by subsectioning each of the cores, in a lN$_2$ bath, into chunks weighing approximately 1 g. Several of these chunks were placed in a cold (77 K) glass test tube fitted at one end with a ground-glass vacuum joint. The tube containing the sample (77 K) was placed on the vacuum line at the entrance port of the gas analyzer. The calibrated needle valve at the entrance port of the high-vacuum system was opened and the tube containing the sample was evacuated. Once the sample pressure reached approximately 5.0 x 10^{-7} mbar the lN$_2$ bath was replaced with an isopentane cryogenic bath (113 K) and the vacuum again applied to the sample. This procedure resulted in the removal of any adsorbed nitrogen and non-enclathrated gases. The needle valve was closed, the cryogenic bath removed, and pressure allowed to build up in the glass tube as the sample dissociated. As the sample temperature approached 273 K, the ice was observed to melt, and this was taken as good evidence that the gas hydrate had dissociated completely. The gas was slowly bled into the high-vacuum system and gas analyzer in a controlled manner by slowly opening the needle valve. The data were recorded as a function of the atomic mass number of each fragment.

Table 2. Precision gas analysis.

Sample (decomposition temperature)	Gas compostion		
	16 AMU	28 AMU	44 AMU
A1 (233 K)	present	present	present
A2 (195 K)	present	absent	absent
A4 (extremely low gas content)			
A5 (221 K)	present	present	present
A6 (220 K)	present	present	present
B1 (210 K)	present	present	present
B2 (193 K)	present	absent	absent
B3 (2 step)	present	present	present
B4 (197 K)	present	absent	absent
B5 (199 K)	present	absent	absent
B6 (219 K)	present	present	present
AMU - atomic mass units			

The guest gases are predominantly composed of methane; however, some samples do show significant quantities of other, heavier gases. The patterns from two typical samples, A2 and B1, are shown in Figure 3a and b. The region between 12 and16 AMU, with the 16 AMU fragment as the major component, is typical of methane. Nitrogen shows fragments at 14 and 28 (major) AMU; however it is unlikely that any nitrogen is present after evacuation of the samples at 113 K. The fragment observed at 44 AMU is known to result from a combination of carbon dioxide and propane (*see* 'Infrared studies of the residual gas content'). Carbon dioxide is known to have fragments at 12, 16, 28, and 44 (major) AMU. A listing of the presence (or absence) of the major fragments in the cracking patterns for all 11 core samples is presented in Table 2 (rough estimates based on vacuum-line gas separation indicate that the methane content is not below 97%, again *see* FTIR results below). The sample naming scheme reflects that of Table 1 and the bracketed values quoted after the sample name indicate the approximate decomposition temperature (±3 K) as determined from the decomposition profiles given in Figure 2 and the method described above. Sample A4 did not contain enough gas to measure and sample B3 exhibited a two-step decomposition profile. The general trend seems to be that samples containing only methane begin to

decompose at lower temperature, while those which also contain heavier gases are slightly more stable and begin to decompose at higher temperature.

DETAILED ANALYSIS

Initial powder X-ray diffraction experiments were attempted on samples containing gas hydrate, ice, and background sand matrix (i.e. without concentrating the gas hydrate phase). It was discovered quickly that the gas hydrate component of the samples was too low. The identifiable diffraction reflections resulted from SiO_2, and some very weak ice I reflections were apparent, but there was no indication of gas hydrate content. It was decided that the gas hydrate must be concentrated for successful molecular-level analysis, and two samples with high gas content were selected as good candidates for the separation procedure. The first was sample A2, which contained 0.50 mmol/g of gas with a decomposition temperature of T = 195 K. The guest species was almost entirely methane without a significant quantity of heavier gas (*see* Fig. 3a). The second was sample B1, which contained 0.19 mmol/g of gas with a decomposition temperature of T = 210 K; again the guest species is almost entirely methane, but some heavier gases were present (Fig. 3b).

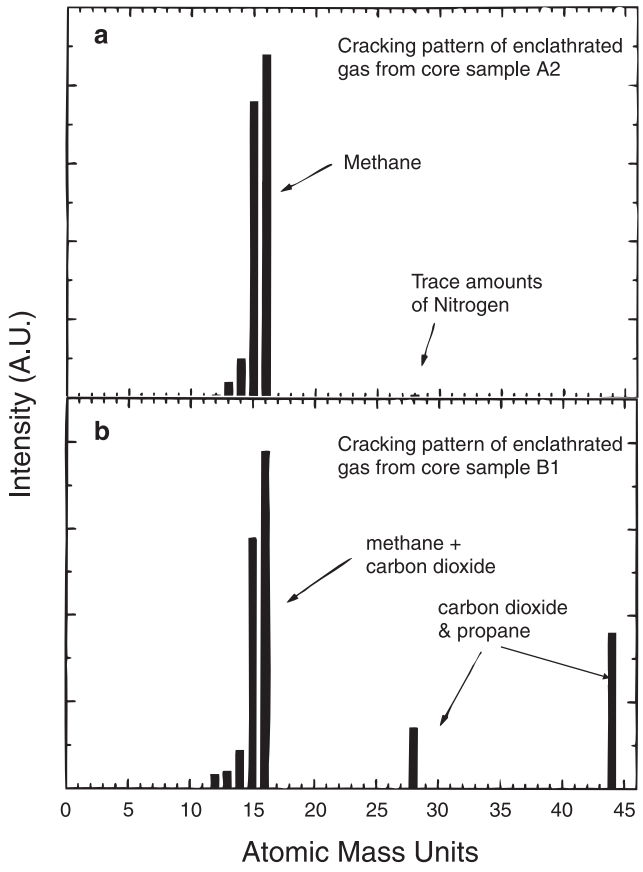

Figure 3. *Precision gas analysis of the gases from core samples A2 and B1. The cracking pattern of gas collected from core sample A2 shows that the enclathrated species is methane only, while the cracking pattern of gas collected from core sample B1 indicates significant quantities of other heavier guest molecules.*

Sample separation procedure

Since it is likely that most natural gas hydrate is located in the interstitial spaces between grains of consolidated sand, and that concentration of the gas hydrate is necessary for most molecular-scale analytical techniques, the procedure used to separate these components is described in some detail. Samples were removed from lN$_2$ storage, immediately placed in a lN$_2$ bath, and subsectioned into approximately 0.5 g pieces. Several of these pieces were placed into a cold steel mortar placed in the lN$_2$ bath. The sample was then ground into a fine powder with a cold steel pestle, the vigorous grinding separating the ice and gas hydrate from the sand grains. Liquid nitrogen was added to the mortar and the mixture was stirred vigorously with a cold steel spoon. The sand quickly settled to the bottom whereas the much less dense ice–gas hydrate mixture remained suspended in the lN$_2$ for several seconds before settling on top of the sand. After removal of almost all of the lN$_2$ in the mortar, the ice–gas hydrate mixture was collected very carefully from the top of the deposit with the cold spoon. Most of the ice–gas hydrate mixture was separated using this technique. The remaining gas hydrate could be recovered in concentrated form by adding more lN$_2$ to the mortar, rapidly stirring the remaining deposit and then, after the sand had settled, pouring off the ice–gas hydrate suspension before it had settled on the sand. The separated material was then either stored in liquid nitrogen for future studies, or was immediately placed on a copper platform just above the surface of the rapidly boiling nitrogen and allowed to dry.

Infrared studies of the residual gas content

The residual gas species of the gas hydrate concentrated from the B1 core sample (i.e. the heavier component of the enclathrated gas) was identified with gas-phase Fourier transform infrared (FTIR) spectroscopy. Approximately 10 g of core sample were dissociated on a vacuum line as described in the previous section, and the collected gas was stored in a gas bulb. Water vapour collected along with the gas was removed by leaving the gas over a small quantity of P_2O_5 overnight. A cell fitted with sodium chloride infrared windows and designed for use with a BIORAD FTS-40A FTIR spectrometer was filled to 3.2 Torr with the dried nonfractionated gas mixture. The room-temperature spectrum of the gas was obtained by co-adding 256 scans at 2 cm^{-1} resolution. All the spectral bands of the non-fractionated gas mixture can be identified as arising from methane, there being no evidence of another species. This was a good indication that the heavier gases only form a very small portion of the total gas content. In order to proceed with the analysis, the methane component of the gas hydrate gas had to be separated from the heavier gases.

The separation was facilitated by the large difference in vapour pressures of condensed methane (10 Torr) and that of heavier molecules (~ 0 Torr) at liquid-nitrogen temperature.

Therefore, after recording the room-temperature pressure in the vacuum line, the gas was condensed by cooling it to 77 K and the methane pumped away completely (vacuum-line pressure 0 Torr.). The cell subsequently was warmed to room temperature, and the line pressure measured and compared with the previous value. The less volatile components constituted only about 1.5 to 2.0% of the total gas content. The FTIR cell was then filled with the residual gas to 3.2 Torr and the room-temperature IR spectrum was collected under the experimental conditions described above. The absorption spectrum is plotted along with spectra of propane (C_3H_8) and carbon dioxide (CO_2) in Figure 4 and indicates clearly that significant amounts of both are present in the gas hydrate from the B1 core sample.

In order to determine the relative concentration of CO_2 and propane in the residual gas, FTIR spectra for a series of gas mixtures ranging from 0 to 99% CO_2 in propane were recorded to establish a calibration curve. In each absorption spectrum the ratio of the integrated intensity of the propane component at 2973 cm^{-1} to the integrated intensity of the CO_2 component at 2364 cm^{-1} was plotting versus concentration. By integrating the same two peaks in the spectrum of the residual gas, the CO_2 fraction was determined to be 85%.

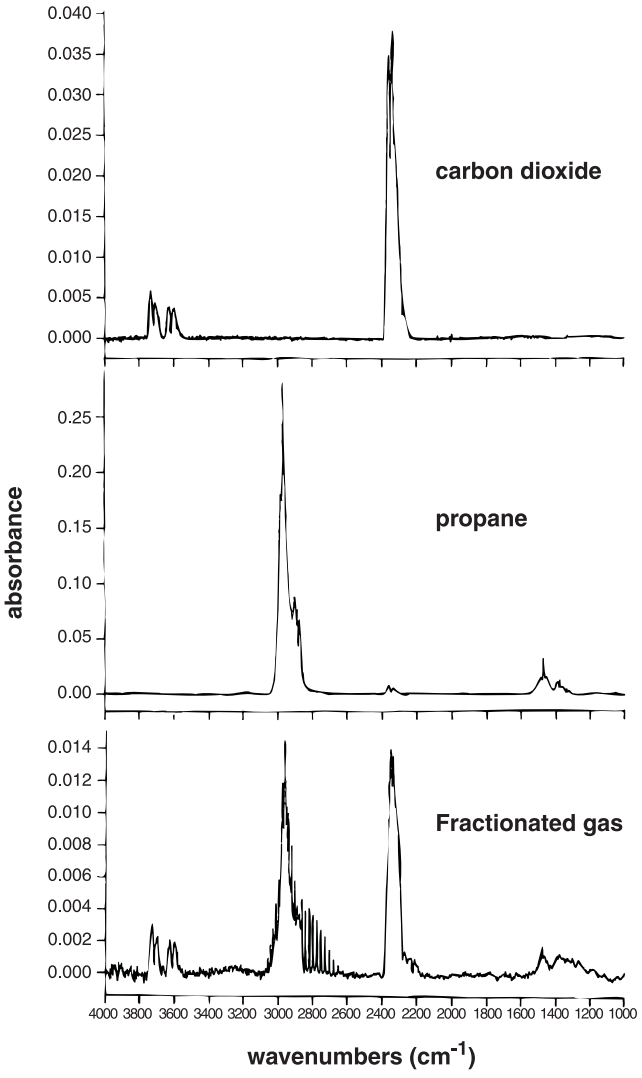

Figure 4. *Fourier transform infrared spectra of the dissociated gas from sample B1. The fractionated sample is compared with propane and carbon dioxide.*

Powder X-ray diffraction

The crystallographic structure of the two concentrated gas hydrate–ice samples, A2 and B1, was determined directly by powder X-ray diffraction at 90 K. The dry gas hydrate–ice concentrate was placed in a cold (77 K) flatbed powder X-ray sample holder. To minimize crystallite orientation effects, extra care was taken to ensure that the surface of the sample was smooth and not tightly packed. The hermetically sealed sample chamber of a Rigaku powder X-ray diffractometer (radiation - MoK_α $\lambda = 1.79021$ Å) was cooled to 90 K with a liquid nitrogen cooling assembly, and the sample was loaded into the diffractometer such that the temperature did not rise above 100 K. A platinum resistance thermometer was placed directly beneath the sample holder and the temperature measured and controlled using a PAAR TTK-HC temperature controller.

Powder diffraction patterns of samples A2 and B1 were collected between $2\theta = 5$ and 40° and are presented in Figure 5a and b, respectively. The structure was identified by calculating the X-ray powder diffraction pattern for each of the known gas hydrate phases (structures I, II, and H) using known structural information and by conducting a detailed comparison with the experimental data. The peaks identified as Structure I gas hydrate are indicated by the Miller indices in Figure 5; the more predominant ice I peaks are indicated by ice Ih (hexagonal); and the peaks identified as arising from the quartz component of the sand are indicated by SiO_2. The low angle peaks (i.e. the [211] reflection and below) indicate a large unit cell and are considered necessary for accurate gas hydrate phase identification. Data collection at a very low 2θ angle results in higher background counts due to the straight-through, undiffracted, X-ray beam and thus data collection below $2\theta = 5°$ was not possible. Therefore, the lowest angle peak observed was the [110] peak at $2\theta = 12.34°$ for sample A2. The reason this peak was not observed in the B1 sample is thought to be a result of lower gas hydrate content (note the ratio of the gas content to percent water content is 0.019 for sample B1 and 0.034 for sample A2, *see* Table 1). Since sample A2 produced the best powder X-ray data, the 2θ value of the experimentally determined peaks are tabulated and compared with the calculated 2θ value (Table 3). All experimental data presented in Table 3 has been corrected for off-axis shift created by thermal contraction of the sample holder. The angular shift parameter δ in the Braggs law formula $\lambda = 2d \sin(\theta + \delta)$, where d is the correct planar spacing, λ is the X-ray wavelength and 2θ is measured diffraction angle, has been calculated using the [111] X-ray reflection of c-Si recorded under the same conditions as the gas hydrate + ice sample. The corrected $2\theta^{cal}$ values given in Table III clearly result from a Structure I gas hydrate lattice, unit cell parameter $a \sim$

Table 3. Powder XRD data.

Peak #	$2\theta^1$ (correct)	$2\theta^2$ (calc)	Miller Indices
1	12.34	12.36	[110]
2	17.59	17.59	[200]
3	19.64	19.60	[210]
4	21.44	21.49	[211]
5	24.52	SiO_2	
6	26.80	Ice Ih	
7	28.51	Ice Ih	
8	30.40	30.58/Ice Ih	[222]
9	31.36	SiO_2	
10	33.07	33.10	[321]
11	36.47	36.57	[410]
12	37.52	37.60	[330]
13	37.87	-	
14	39.52	Ice Ih	

[1] peak positions have been corrected for off-axis shift as described in the text.
[2] calculated peak positions for Structure I clathrate gas hydrate with unit cell size a = 11.75Å

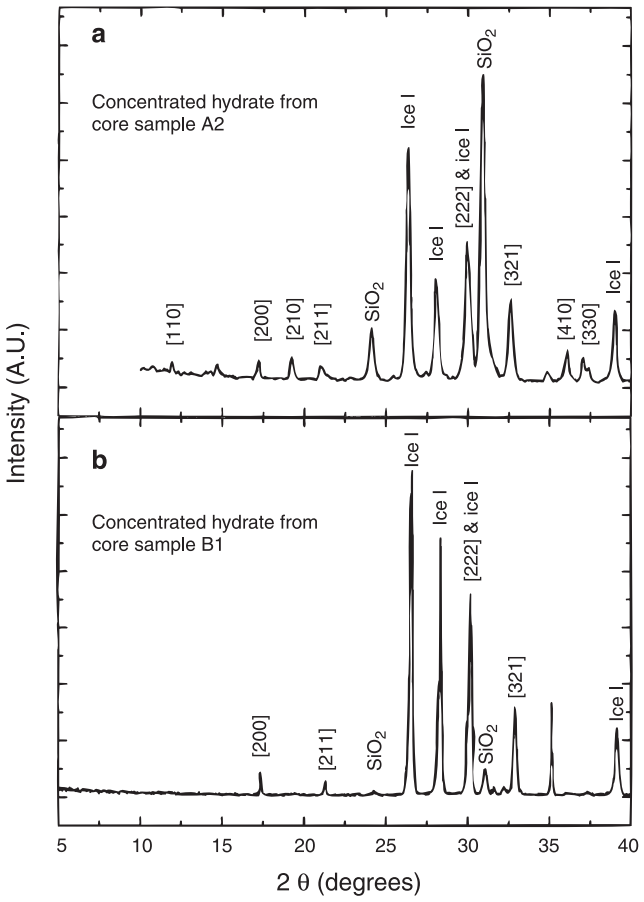

11.75Å, the SiO_2 $2\theta^{cal}$ values resulted from using an hexagonal (space group $P3_1\ 2\ _1$) lattice with a = 4.915 Å and b = 5.406 Å.

The data presented above provide direct evidence that the Mallik 2L-38 samples contain mainly Structure I gas hydrate. Any other gas hydrate structures present occur in quantities too small to be detected directly in this experiment. It is worth noting at this point that the approximate composition values for pure methane gas hydrate is $CH_4 \cdot 6\ H_2O$ (Davidson, 1973).

Thermal analysis of the decomposition process

Accurate values of the decomposition temperature, enthalpies of dissociation, and heat capacities of pure laboratory-produced methane, ethane, propane, and isobutane gas hydrate have been measured (Handa, 1986; Handa and Stupin, 1992; Handa et al., 1989, 1997). It was noted that distinct differences exist in the dissociation processes of Structure I and Structure II gas hydrate. In addition, the calorimetric data for the dissociation of natural gas hydrate obtained from the Gulf of Mexico, Ocean Drilling Project (ODP) leg 164 and Deep Sea Drilling Project (DSDP) gas hydrate recovered at site 570, Leg 84 have been compared with those for synthetic gas hydrate (Handa et al., 1997). Thermal traces recorded during the heating cycle of the calorimeter indicated that the DSDP and ODP samples decomposed in a very similar manner to methane gas hydrate and therefore are likely to be Structure I, whereas the Gulf of Mexico samples are Structure II gas hydrate. The heat of decomposition for the laboratory-produced methane gas hydrate at gas/ice/hydrate equilibrium has been measured between 160 and 210 K and found to be 18.13 ± 0.27 kJ/mol.

Evidence for the variability in the equilibrium dissociation temperature, and, indeed more accurate values of the dissociation temperature of the Mallik 2L-38 gas hydrates were investigated for concentrated gas hydrate material obtained from core samples A2 (methane hydrate) and B1 (methane hydrate with significant amounts of propane and CO_2), and low-temperature differential scanning calorimetry (DSC). The gas hydrate–ice samples were concentrated from 10 to 15 g of recovered core samples A2 and B1 and are therefore thought to represent a core sample average. The TA Instruments 2920 DSC calorimeter was calibrated for low temperature and heat flow with the melting transition of mercury and corrections for the temperature lag of the instrument and baseline offset were made automatically using the data-analysis software.

Figure 5. *X-ray powder diffraction pattern of the concentrated hydrate + ice collected from core sample A2* ***(a)****, and B1* ***(b)****. The reflection at 2θ~35.4° in (b) roughly corresponds with the reflection from the Structure II gas hydrate [531] crystallographic plane ($2\theta^{cal}$ = 35.73°). However, since no other peaks arising from Structure II gas hydrate appear, especially in the low-angle region, definite phase identification cannot be made. (This peak may well result from some unidentified crystalline material in the sample.)*

Dry concentrated samples were placed in cold (77 K) aluminum hermetic DSC pans and were sealed using a specially designed press that was cooled to 77 K in a lN$_2$ bath. The press was designed in such a way that the pan was held just above the surface of rapidly boiling lN$_2$. It is known from previous experiments that the sample temperature did not rise above 100 K during the sealing process. Once the sample was sealed, the DSC sample chamber containing the reference pan only was cooled to 123 K and held isothermally until the sample was completely loaded. A liquid-nitrogen dewar was designed to fit over the entrance to the DSC sample chamber in order to provide a dry atmosphere of cold nitrogen gas. The sample chamber lids were removed and the sample carefully put in place. The lids were replaced and the samples were held isothermally for at least 10 min to allow the instrument to regain equilibrium and to allow the helium purge gas to displace the nitrogen gas in the sample chamber. It is critically important that significant amounts of water do not condense onto the sample pan during the sealing and loading process. Rapidly boiling lN2 provided a dry atmosphere that was sufficiently free from atmospheric water. As a test, an empty pan was sealed and loaded into the DSC sample chamber following the exact method used for the concentrated gas hydrate samples. An ice melting endotherm near 273 K was not evident.

The sample temperature was then raised at 5 K/min from 123 K to 293 K and the thermal trace recorded. The portion of the traces showing the gas hydrate decomposition endotherm are shown in Figure 6 for samples A2 and B1 respectively. (Desorption of nitrogen has been identified in previous experiments as a large endotherm at the beginning of the trace, but this was not observed in these experiments.) It is evident that the decomposition temperatures of these two gas hydrate samples are somewhat different. The concentrated gas hydrate from the core sample B1, which contains propane and carbon dioxide, decomposes at 208 K and is more stable then the concentrated gas hydrate from core sample A2, which has no detectable heavy gas content (gas analysis results) and decomposes at 193 K. This is in good agreement with the gas-release data presented in the previous section.

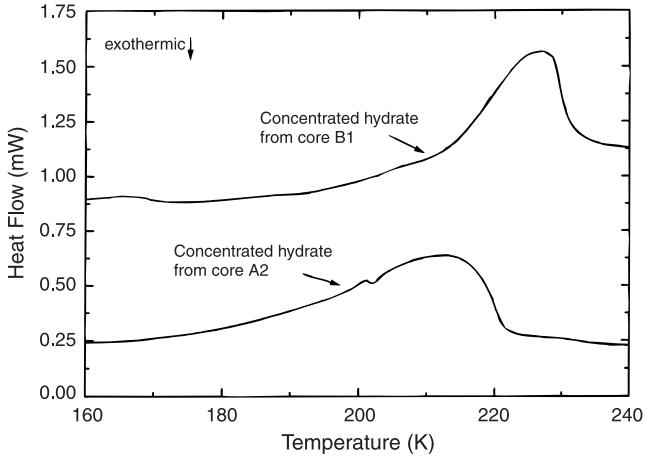

Figure 6. *Differential scanning calorimetry traces of the process of decomposition; the sample mass used was approximately 5 mg. The ice melting lines are not shown.*

Raman spectroscopic studies

Raman spectra arising from the C-H symmetric stretch of enclathrated methane and the coupled O-H stretch of the clathrate host lattice + ice were collected. Previously, it was shown that the methane C-H stretch bands in the large and small Structure I cages are resolvable (Seitz et al., 1987), and some attempts have been made to determine the cage occupancies based on the Raman spectral intensities. This makes use of the equation relating the cage occupancies to the difference in chemical potential of the empty host-water lattice with respect to ice at the three-phase equilibrium point (Sum et al., 1997). There are, however, some questions about the band assignments and intensities, and, therefore, the validity of the use of the ratio of the integrated band intensities to determine the relative cage occupancies and hydration number. Classically, the problem can be described by the fact that the Raman spectral intensity is a result of the interaction of the electromagnetic field of the incident laser light and the polarizability tensor of the scattering molecule (Long, 1977). The electric fields inside the large and small clathrate cages (environments of different symmetry) have not been analyzed, thus the interactions between the host and guests are also not well understood and it is not known if there are differences in the polarizability of the methane in the two cages. The interactions of the guest molecules with the host must be considerable. This fact is reflected first of all by the presence of different C-H stretch frequencies, and also by the large coefficient of thermal expansion (Tse et al., 1987). In addition, the coupling of the motion of the guest molecule within the cage structure with the host lattice vibrations is very important to the acoustic vibrational modes of the crystal and is related to the anomalous glass-like thermal-transport properties of clathrate materials in general (Tse et al., 1993; Tse, 1994). We can conclude that the scattering cross-section of methane in the large and small cage likely is different, making a direct comparison of the integrated intensities difficult. The band assignment problem is illustrated by the fact that the Raman shift resulting from the C-H stretch of methane in what is suggested to be the small cage, 2916 cm^{-1}, seems to be closer to that of methane vapour, 2917 cm^{-1}, than the Raman shift of what is suggested to be the large cage, 2904 cm^{-1}. However, based on experiments with gas mixtures, this assignment seems to be correct (Sum et al., 1997). It is reasonable to expect that the intensity of each Raman band is somehow related to the occupancies of the large and small cages, and therefore comparison of the integrated intensities of the Mallik 2L-38 samples with those for high-quality synthetic methane hydrate will provide some qualitative insight into the cage occupancies. Furthermore, comparison of the intensities of these bands with ^{13}C nuclear magnetic resonance (NMR) data collected from the same samples will help answer many of these questions.

The spectral intensities of the Raman bands resulting from the C-H vibrations of enclathrated methane in the Mallik 2L-38 samples will be compared with those for

synthetic methane hydrate produced under gas/ice/hydrate equilibrium conditions. The Raman spectrum for this sample (T = 10 K) has been reproduced in Figure 7a, *see* below for experimental details. As noted above, such a comparison does provide some qualitative information regarding the occupancy of the large and small cages of the A2 core gas hydrate, and the B1 core gas hydrate, which contains quantities of propane/CO_2 and methane hydrate.

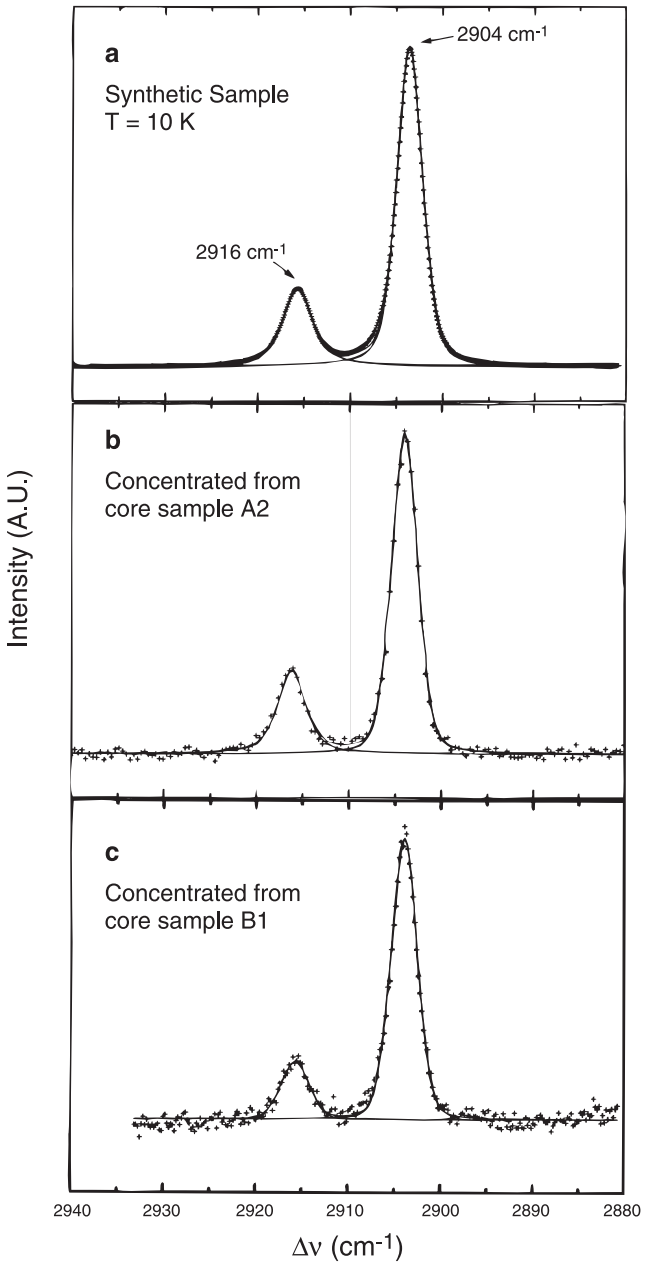

Figure 7. *Raman spectra of the C-H symmetric stretching vibration of methane (v_1) in synthetic hydrate* ***(a)****, hydrate concentrated from core sample A2* ***(b)****, and hydrate concentrated from core sample B1* ***(c)****. The plus signs represent the experimental data and the solid curves represent the fitted pseudo-Voight functions.*

The powdered samples used for Raman experiments were dried above boiling liquid nitrogen for approximately 30 min before being loaded into a cold (77 K) sample holder that could be fitted onto the cold (77 K) cryotip of an Air-Products closed cycle refrigerator. The temperature was monitored (±1 K) with a gold-iron thermocouple located between the cryotip and the sample holder. The rather complicated sample loading process has been discussed in a previous article and the details will not be reviewed here (Tulk et al., 1998). Once the radiation shield and vacuum shroud were placed over the cryotip, the sample temperature decreased to 12 K at a rate of approximately 5 K/min (the sample temperature did not rise above 100 K, and thus no significant annealing of the water framework occurred).

Laser light was provided by an Inova 90-4 argon ion laser at 488 nm and was incident on the sample after being reflected through an optical port in the vacuum shroud opposite the sample. Light scattered from the sample at 180° was collected using f/1.8 optics and passed through a polarization scrambler before being focused on the entrance slits of a SPEX 1403 double monochromator. The slits were set to 200 µm giving a spectral resolution of 1 cm^{-1}. The monochromator was calibrated with the neon emission lines in the spectral region of interest. The minimum operating power of the laser (150 mW) was found to be too high and absorption by other, most likely organic, contaminants resulted in sample damage and complete absence of a Raman signal. Therefore, a Glan-Thompson polarizer was placed between the laser and the sample to reduce the incident laser power to approximately 80 mW. Because of the absorption of laser light, which resulted in sample heating, the sample temperature at the scattering point is not known accurately. The linewidth for the synthetic gas hydrate, however, has been studied in the absence of such laser-light absorption as a function of temperature between 10 and 120 K. Significant line broadening was not observed to occur until T = 100 K, where the full width at half maximum (FWHM) of the 2904 cm^{-1} Raman line was measured to be 4.0 cm^{-1}. Comparatively, the FWHM of the 2904 cm^{-1} Raman line from the Mallik 2L-38 samples was found to be 3.4 cm^{-1}, indicating the local sample temperature at the focal point of the laser to be less than 100 K, well below the decomposition temperature. Polarization analysis of the incident or the scattered light was not performed.

The Raman spectra of the C-H stretching vibrations of enclathrated methane from core samples A2 and B1 are shown in Figure 7b and c, respectively. The two distinct Raman bands can easily be identified at 2904 cm^{-1} and 2916 cm^{-1}, and, due to the benefit of the sharp lines resulting from the low sample temperature (full width at half maximum of Raman line at 2904 cm^{-1} is 3.4 cm^{-1} and that of the Raman line at 2916 cm^{-1} is 3.7 cm^{-1}), the two lines are very well resolved. To help determine the integrated intensities, pseudo-Voight line shapes were fitted to each of the lines in each spectrum. The smooth curves shown in Figure 7 represent the fitted pseudo-Voight functions and the '+' represent the experimental data. From the fitted curves, the ratio of the integrated intensities (I_{2904}/I_{2916}) of the Raman spectrum collected for the synthetic methane hydrate sample was

calculated to be 3.16. (Using previous band assignments (Sum et al., 1997) and taking into consideration that there are three times as many large cages as small cages in the structure I unit cell, the occupancy ratio of the artificial sample would be $\theta_S/\theta_l = 0.95$. This number is in fair agreement with such ratios determined by other methods, for example, NMR studies (Ripmeester and Ratcliffe, 1988) have shown that $\theta_S/\theta_l = 0.92 \pm 0.01$). Similarly, values for the integrated intensity of the concentrates from the core samples A2 and B1 can be calculated. The ratio of the integrated intensities of the A2 core sample gas hydrate was found to be $I_{2904}/I_{2916} = 3.19$ using the fitted curves (considering the difference in the numbers of cages in the unit cell, $\theta_S/\theta_l = 0.94$). Often, fitting curves to such noisy data can give misleading results; therefore, since the two lines are almost completely resolved, the experimental data itself has been integrated as a check of the intensities determined from the fits, and I_{2904}/I_{2916} was found to be 3.26 (or $\theta_S/\theta_l = 0.92$). Considering possible variations in the formation conditions between the synthetic sample and the natural sample, the A2 data agrees very well with the data from the synthetic sample. The ratio of the integrated intensities for gas hydrate from the B1 core, predominantly methane hydrate with low quantities of propane and carbon dioxide, is somewhat different, $I_{2904}/I_{2916} = 3.89$ (or $\theta_S/\theta_l = 0.77$). Again these results have been verified by integrating the experimental data and $I_{2904}/I_{2916} = 4.11$ (or $\theta_S/\theta_l = 0.73$). This is considerably lower than that for pure methane hydrate and provides strong evidence that in the case of core sample B1 either Structure I gas hydrate has formed in the presence of the other guests gases, thus replacing some of the methane from the clathrate cages, or, some Structure II gas hydrate is present with propane in the large cages, thus changing the overall experimental occupancy ratios observed by Raman spectroscopy. As discussed above, the propane and carbon dioxide constitute only 2.0% of the total enclathrated gas, and at this level these gas species cannot be detected using Raman spectroscopy. Propane-methane mixtures have been shown to form Structure II gas hydrate when the propane concentration is higher then about 2% (van der Waals and Platteeuw, 1959). Low concentrations of Structure II gas hydrate may well be undetectable using the X-ray diffraction technique described above and thus could easily be overlooked. It is worth speculating that the first case is unlikely because the methane would be displaced from the large cage by either propane or carbon dioxide. This would cause the Raman band ratio to increase rather than decrease (i.e. the number of methane molecules in the small Structure I cage relative to the number in the large cage would increase). If some Structure II gas hydrate was stabilized by the presence of propane molecules in large cages, then methane would still be concentrated in the small cages of both Structure I and Structure II gas hydrate. At this stage it is difficult to see how the band ratio could decrease, as both of the possible explanations would require the opposite behaviour. However, this could be evidence that the 2904 cm^{-1} line could result from the small cage and the 2916 cm^{-1} line could result from the large cage.

Without further scientific studies and more fundamental understanding of all the processes involved, caution should be used when applying Raman spectroscopy to extract quantitative occupancy information from gas hydrate. Raman spectroscopy has, however, been used here for the first time to extract qualitative molecular-level occupancy information from naturally occurring gas hydrate. It was the Raman data that first suggested that the heavier gas component might be responsible for the stability variation observed during dissociation.

CONCLUSIONS

Eleven core samples collected from the JAPEX/JNOC/GSC Mallik 2L-38 research well drilled on the Mackenzie Delta have been evaluated. In the first part of the study, the entire core samples, background sand matrix + gas hydrate + ice, were studied. Initial visual inspection revealed core samples from the Mallik site show little or no visible gas hydrate material. Later analysis indicated that, on average, 85% of the core was composed of the background sand matrix. In fact, the gas volume and water content analyses indicate that most of the material that appears to be gas hydrate is ice. The gas content and stability of the gas hydrate material were studied, and the enclathrated gas species present were partially identified. It should be noted that the gas hydrate content in the sample studied in the laboratory is likely to be far less than what it is in the ground. Significant amounts of the gas hydrate probably are lost during the recovery of the cores. Therefore, direct comparison of the gas hydrate content found here with the in situ gas hydrate content is very difficult without a detailed knowledge of the thermal processes during core extraction. In order to facilitate molecular-level studies, the second portion of this study involved identifying two samples with high gas hydrate content, but with slightly different gas composition and concentration of the gas hydrate. The molecular-scale properties of concentrated samples were then studied by powder X-ray diffraction, calorimetry, and Fourier transform infrared and Raman spectroscopy.

When combined, the experimental techniques used indicated a large heterogeneity in both the distribution and stability of the gas hydrate among various core samples and, in some cases, considerable variation within individual core subsamples (*see* for example the dissociation characteristics of core sample B3, above). While such heterogeneity may have resulted during the core-recovery process, the experimental techniques nonetheless have been designed to provide a representative analysis of the whole core sample (*see* discussion in text).

Most of the enclathrated gas was methane; however, some samples did show approximately 1.5–2.0% of a propane/carbon dioxide gas mixture. The powder X-ray diffraction analysis showed conclusively that the bulk of the gas hydrate was Structure I. In addition, there seemed to be a correlation between the presence of the heavier gas molecules and the stability of the gas hydrate material. The variation in dissociation temperature was evident from both the gas volume and dissociation studies. This was further verified by the DSC studies of the concentrated gas hydrate from core samples A2 and B1; the correlation with the heavier gas component is evident from the qualitative analysis of the cracking patterns of

the precision mass analyzer and the FTIR gas spectroscopic studies. However, to date no technique has clearly indicated whether the propane and carbon dioxide result in a mixture of structures, a mixture of components, or a combination of both. Considering the sample handling before data collection, it is highly unlikely that the small quantities of carbon dioxide and propane are simply gas inclusions that do not form part of the clathrate structure. Therefore, it is clear that any model gas hydrate systems that are proposed for the Mallik 2L-38 well should include small quantities of both these gases.

Finally, the occupancy ratios of the gas hydrate cages have been investigated qualitatively and a comparison with synthetic pure methane hydrate indicates that perhaps some of the propane and carbon dioxide molecules displace the methane. One very interesting, and yet unresolved, observation is that the occupancy ratio (small cages to large cages) of the mixed gas hydrate samples appears to decrease rather than increase when the larger propane and CO_2 molecules are included. This is opposite to what would be expected on displacement of the methane from the large cages of either Structure I or II by propane or CO_2.

ACKNOWLEDGMENTS

The core samples were collected, cared for, and transported to NRC by F.M. Nixon, J.F. Wright, S.R. Dallimore, and L.R. Snowdon of the Geological Survey of Canada. R. Dutrisac, and Y. Yuan assisted with the collection of experimental data at NRC, also S. Okada provided many helpful suggestions. The authors would also like to acknowledge the Geological Survey of Canada and the Japan Petroleum Exploration Company for providing financial support.

NRCC no.: 40912

REFERENCES

Davidson, D.W.
1973: Clathrate hydrates; *in* Water. A Comprehensive Treatise, (ed.) F. Franks; Plenum, New York, New York, p. 115–234.

Davidson, D.W., Garg, S.K., Gough, S.R., Handa, Y.P., Ratcliffe, C.I., Ripmeester, J.A., Tse, J.S., and Lawson, W.F.
1986: Laboratory analysis of a naturally occurring gas hydrate from sediment of the Gulf of Mexico; Geochima et Cosmochima Acta, v. 50, p. 619–623.

Handa, Y.P.
1986: Compositions, enthalpies of dissociation, and heat capacities in the range 85 to 270 K for clathrate hydrates of methane, ethane, and propane, and enthalpy of dissociation of isobutane hydrate, as determined by a heat-flow calorimeter; Journal of Chemical Thermodynamics, v. 18, p. 915–921.

Handa, Y.P. and Stupin, D.
1992: Thermodynamic properties and dissociation characteristics of methane and propane hydrates in 70 Å-radius silica gel pores; Journal of Physical Chemistry, v. 96, p. 8599–8603.

Handa, Y.P., Wong, B., Krzymien, M., McLaurin, G., Darren, B., Tse, J.S., and Ripmeester, J.A.
1997: Thermophysical and structural characterization of naturally occurring gas hydrates from Blake Ridge and the Gulf of Mexico; *in* Proceedings of the International Workshop on Gas Hydrates, 2nd Joint Japan–Canada Workshop, Tsukuba, Japan, p. 154.

Handa, Y.P., Yamamuro, O., Oguni, M., and Suga, H.
1989: Low-temperature heat capacities of xenon and krypton clathrate hydrates; Journal of Chemical Thermodynamics, v. 21, p. 1249.

Jeffrey, G.A.
1996: Hydrate inclusion compounds; *in* Comprehensive Supramolecular Chemistry, (ed.) J.L. Atwood, J.E.D. Davis, D.D. MacNicol, F. Vögtle, Elsevier, New York, New York, v. 6 p 757–788.

Kvenvolden, K.A.
1994: Natural gas hydrate occurrence and issues; Annals of the New York Academy of Science, v. 715, p. 232.

Long , D.A.
1977: Raman spectroscopy, McGraw-Hill: New York, New York, 271 p.

Ripmeester, J.A. and Ratcliffe, C.I.
1988: Low-temperature cross-polarization/magic angle spinning ^{13}C NMR of solid methane hydrates: structure, cage occupancy and hydration number; Journal of Physical Chemistry, v. 92, p. 337–339.

Ripmeester, J.A., Ratcliffe, C.I., Klug, D.D., and Tse, J.S.
1994: Molecular perspectives on structure and dynamics in clathrate hydrates; Annals of the New York Academy of Science, v. 715, p. 161–176.

Ripmeester, J.A., Tse, J.S., Ratcliffe, C.I., and Powell, B.M.
1987: A new clathrate hydrate structure; Nature, v. 325, p. 135–136.

Sassen, R. and MacDonald, I.R.
1994: Evidence of structure H hydrate, Gulf of Mexico continental shelf; Organic Geochemistry, v. 22, p. 1029–1032.

Seitz, J.C., Pasteris, J.D., and Wopenka, B.
1987: Characterization of CO_2-CH_4-H_2O fluid inclusions by microthermometry and laser Raman microprobe spectroscopy: inferences for clathrate and fluid equilibria; Geochimica et Cosmochimica Acta, v. 51, p.1651–1664.

Sloan, E. D.
1998: Clathrate hydrates of natural gas, Marcel Dekker, New York, New York, 705 p. (second edition).

Sum, A.K., Burruss, R.C., and Sloan, E.D.
1997: Measurement of clathrate hydrates via Raman spectroscopy; Journal of Chemical Physics B., v. 101, p. 7371–7377.

Tse, J.S.
1994: Dynamical properties and stability of clathrate hydrates; Annals of the New York Academy of Sciences, v. 715, p. 187–206.

Tse, J.S., McKinnon, W.R., and Marchi, M.
1987: Thermal expansion of structure I ethylene oxide hydrate; Journal of Physical Chemistry, v. 91, p. 4188–4193.

Tse, J.S., Powell, B.M., Sears, V.J. , Handa, Y.P.
1993: The lattice dynamics of clathrate hydrates: an incoherent neutron scattering study; Chemical Physics Letters, v. 215, p. 383–387.

Tulk, C.A., Klug, D.D., Branderhorst, R., Sharpe, P., and Ripmeester, J.A.
1998: Hydrogen bonding in glassy liquid water from Raman spectroscopic studies; Journal of Chemical Physics, v. 109, p. 8478–8484.

Tulk, C.A., Wright, J.F., Ratcliffe, and C.I., Ripmeester, J.A.
1999: Storage and handling of natural gas hydrate; *in* Scientific Results from JAPEX/JNOC/GSC Mallik 2L-38 Gas Hydrate Research Well, Mackenzie Delta, Northwest Territories, Canada, (ed.) S.R. Dallimore, T. Uchida, and T.S. Collett; Geological Survey of Canada, Bulletin 544.

Udachin, K.A., Ratcliffe, C.I., Enright, G.D., and Ripmeester, J.A.
1997: Structure H hydrate: a single crystal diffraction study of 2,2-dimethylpentane•5(Xe,H_2S)•34H_2O; Supramolecular Chemistry, v. 8, p.173–176.

van der Waals, J.H. and Platteeuw, J.C.
1959: Clathrate solutions; *in* Advances in Chemical Physics volume II, (ed.) I. Prigogine; Interscience Publishers, New York, New York, p.1–58.

Wright, J.F., Dallimore, S.R., Nixon, F.M., Uchida, T., Winters, W.J., and Collett, T. S.
1999: Influences of grain size and salinity on pressure-temperature thresholds for methane hydrate stability in JAPEX/JNOC/GSC Mallik 2L-38 gas hydrate research well; *in* Scientific Results from JAPEX/JNOC/GSC Mallik 2L-38 Gas Hydrate Research Well, Mackenzie Delta, Northwest Territories, Canada, (ed.) S.R. Dallimore, T. Uchida, and T.S. Collett; Geological Survey of Canada, Bulletin 544.